Downloaded from orbit.dtu.dk on: May 05, 2023

DTU Library

Optofluidic microscope with 3D spatial resolution

Vig, Asger Laurberg; Marie, Rodolphe; Jensen, Eric; Kristensen, Anders

Published in:
Optics Express

Link to article, DOI:
10.1364/OE.18.004158

Publication date:
2010

Document Version
Publisher's PDF, also known as Version of record

Link back to DTU Orbit

Citation (APA):
Vig, A. L., Marie, R., Jensen, E., & Kristensen, A. (2010). Optofluidic microscope with 3D spatial resolution. *Optics Express*, *18*(5), 4158-4169. https://doi.org/10.1364/OE.18.004158

General rights
Copyright and moral rights for the publications made accessible in the public portal are retained by the authors and/or other copyright owners and it is a condition of accessing publications that users recognise and abide by the legal requirements associated with these rights.

- Users may download and print one copy of any publication from the public portal for the purpose of private study or research.
- You may not further distribute the material or use it for any profit-making activity or commercial gain
- You may freely distribute the URL identifying the publication in the public portal

If you believe that this document breaches copyright please contact us providing details, and we will remove access to the work immediately and investigate your claim.

Optofluidic microscope with 3D spatial resolution

Asger Laurberg Vig, Rodolphe Marie, Eric Jensen and Anders Kristensen*

DTU Nanotech – Department of Micro and Nanotechnology, Technical University of Denmark, Building 345east, Ørsteds Plads, DK-2800 Kongens Lyngby, Denmark

*anders.kristensen@nanotech.dtu.dk

Abstract: This paper reports on-chip based optical detection with three-dimensional spatial resolution by integration of an optofluidic microscope (OFM) in a microfluidic pinched flow fractionation (PFF) separation device. This setup also enables on-chip particle image velocimetry (PIV). The position in the plane perpendicular to the flow direction and the velocity along the flow direction of separated fluorescent labeled polystyrene microspheres with diameters of 1 μm, 2.1 μm, 3 μm and 4 μm is determined by the OFM. These results are bench marked against those obtained with a PFF device using conventional fluorescence microscope readout. The size separated microspheres are detected by OFM with an accuracy of $\leq$0.92μm. The position in the height of the channel and the velocity of the separated microspheres are detected with an accuracy of 1.4 μm and 0.08 mm/s respectively. Throughout the measurements of the height and velocity distribution, the microspheres are observed to move towards the center of the channel in regard to its height.

© 2010 Optical Society of America

OCIS codes: (110.0180) Microscopy; (110.2970) Image detection systems; (110.4235) Nanolithography; (120.1880) Detection; (130.3990) Micro-optical devices; (220.4000) Microstructure fabrication; (220.4241) Nanostructure fabrication.

References and links

1. S. Balslev, A. M. Jorgensen, B. Bilenberg, K. B. Mogensen, D. Snakenborg, O. Geshke, J. P. Kutter, and A. Kristensen, "Lab-on-a-chip with integrated optical transducers," Lab Chip **6,** 213–217 (2006).
2. T. L. Olesen, B. B. Buus, J. G. Howalt, and M. F. Hansen, "Magnetic micromixer: Influence og magnetic element geometry and field amplitude," Appl. Phys. **103,** 07E902 (2008).
3. N. Pamme, "Continous flow separation in microfluidic devices," Lab Chip **7,** 1644–1654 (2007).
4. D. Janasek, J. Franzke, and A. Manz, "Scaling and design of miniaturized chemical-analysis systems," Nature **442,** 374–380 (2006).
5. A. Manz, J. C. Fettinger, E. Verpoorte, H. Ldi, H. M. Widmer, and D. J. Harrison, "Micromachining of monocrystalline silicon and glass for chemical analysis systems - A look into next century's technology or just a fasionable craze," Trends Anal. Chem. **10,** 144–149 (1991).
6. X. Heng, D. Erickson, L. R. Baugh, Z. Yaqoob, P. W. Sternberg, D. Psaltis, and C. Yang, "Optofluidic microscopy - a method for implementing a high resolution optical microscope on a chip," Lab Chip **6,** 1274–1276 (2006).
7. X. Cui, L. M. Lee, X. Heng, W. Zhong, P. W. Sternberg, D. Psaltis, and C. Yang, "Lensless high-resolution on-chip optofluidic microscopes for Caenorhabditis elegans and cell imaging," Proc. Natl. Acad. Sci. U.S.A. **105,** 10670–10675 (2008).
8. X. Heng, E. Hsiao, D. Psaltis, and C.Yang, "An optical tweezer actuated, nanoaperture-grid based Optofluidic Microscope implementation method," Opt. Express **15,** 16367–16375 (2007).
9. R. Lindken, M. Rossi, S. Große, and J. Westerweel, "Micro-particle Image Velocimetry (μPIV): Recent developments, applications, and guidelines," Lab Chip **15,** 2551–2567 (2009).
10. M. Yamada, M. Nakashima, and M. Seki, "Pinched Flow Fractionation: Continous Size Separation of Particles Utilizing a Laminar Flow Profile in a Pinched Microchannel," Anal. Chem. **76,** 5465–5471 (2004).

#118773 - $15.00 USD Received 22 Oct 2009; revised 8 Feb 2010; accepted 11 Feb 2010; published 17 Feb 2010

11. J. Takagi, M. Yamada, M. Yasuda, and M. Seki, "Continous particle separation in a microchannel having asymmetrically arranged multiple branches," Lab Chip **5,** 778–784 (2005).
12. Y. Sai, M. Yamada, M. Yasuda, and M. Seki, "Continous separation of particles using a microfluidic device equipped with flow rate controle valves," J. Chromatogr. A **1127,** 214–220 (2006).
13. H. Maenaka, M. Yamada, M. Yasuda, and M. Seki, "Continous and Size-Dependent Sorting of Amulsion Droplets Using Hydrodynamics in Pinched Microchannels," Langmuir **24,** 4405–4410 (2008).
14. A. V. Larsen, L. Poulsen, H. Birgens, M. Dufva, and A. Kristensen, "Pinched flow fractionation devices for detection of single nucleotide polymorphisms," Lab Chip **8,** 818–821 (2008).
15. N. A. Mortensen, "Comment on 'Pinched Flow Fractionation: Contonous Size Separation of Particles Utilizing a Laminar Flow Profile in a Pinched Microchannel'," Anal. Chem. **79,** 9240–9241 (2007).
16. A. L. Vig and A. Kristensen, "Separation enhancement in pinched flow fractionation," Appl. Phys. Lett. **93,** 203507 (2008).
17. B. Bilenberg, M. Hansen, D. Johansen, V. Özkapici, C. Jeppesen, P. Szabo, I. M. Obieta, O. Arroyo, J. O. Tegenfeldt, and A. Kristensen,"Topas-based lab-on-a-chip microsystems fabricated by thermal nanoimprint lithography," J. Vac. Sci. Technol. B **23,** 2944–2949 (2005).
18. J. C. Giddings, *Unified separation science*, (Wiley and Sons, Inc, 1991).
19. K. Yapici, R. L. Powell, and R. J. Phillips,"Particle migration and suspension structure in a steady and oscillatory plane Poiseuille flow," Phys. Fluids **21,** 053302 (2009).

1. Introduction

Microfluidic systems with integrated units such as waveguides, lasers [1], mixers [2] and separators [3] have proven to be ideal tools for precise handling of small biological and chemical samples, enabling fast analysis in point-of-care and research perspectives [4, 5]. The main idea of these systems is that they should be easy-to-use, cheap, compact and portable. However, bulky and expensive optical microscopes are commonly used with the microfluidic systems, especially in analysis of biological and chemical samples.

One alternative is the optofluidic microscope (OFM) [6] which is a cheap, compact and more automated choice in regards to retrieving data. Furthermore, the OFM is implementable in microfluidic platforms and is therefore also portable. The OFM consist of an opaque film patterned with apertures arranged in a line which is tilted relative to the flow direction of an above lying microfluidic channel. Time resolved transmission of light through the apertures as well as knowledge of the laminar flow velocity is used to reconstruct the image of a passing object, at a resolution defined by the dimensions of the aperture array. In the pioneering article by Heng et al. [6], the OFM was demonstrated in combination with a conventional microscope, which was used as a relay. This approach is also used in the present article. For a portable system the OFM must be fabricated directly on top of a lens array and a CCD or CMOS detector, which has been demonstrated by Cui et al. [7]. The OFM has been applied for imaging of Caenorhabditis elegans and cells with a resolution below 1 μm [7] and a resolution down to 110 nm with a grid design has been reported [8]. The largest challenge with OFM is tumbling of sample objects. The grid design mentioned above is one of the ways to deal with the problem, but still images of tumbling particles, which counts up to 40 %, are discarded.

In this article we demonstrate optical detection with 3-dimensional (3D) resolution of size separated microspheres as well as particle image velocimetry (PIV) [9] by OFM. The OFM is integrated into a microfluidic size separation device based on pinched flow fractionation (PFF) [10], positioned under the so called broadening segment, as illustrated in Fig. 1(a). PFF is chosen as a model separation system because it has a good stability and a channel layout which is well suited for integration with the OFM. In addition, tumbling is insignificant in PFF and usually spherical particles are separated. By choosing the OFM technology for positioning readout in PFF, tumbling is therefore not an issue, which is a clear advantage compared to earlier demonstrations of the OFM. PFF has been applied for separation of erythrocytes from blood [11], separation of sub-micrometer sized microspheres [12], size-dependent sorting of emulsion droplets [13] and recently we demonstrated PFF as a DNA analysis technique

#118773 - $15.00 USD Received 22 Oct 2009; revised 8 Feb 2010; accepted 11 Feb 2010; published 17 Feb 2010
(C) 2010 OSA

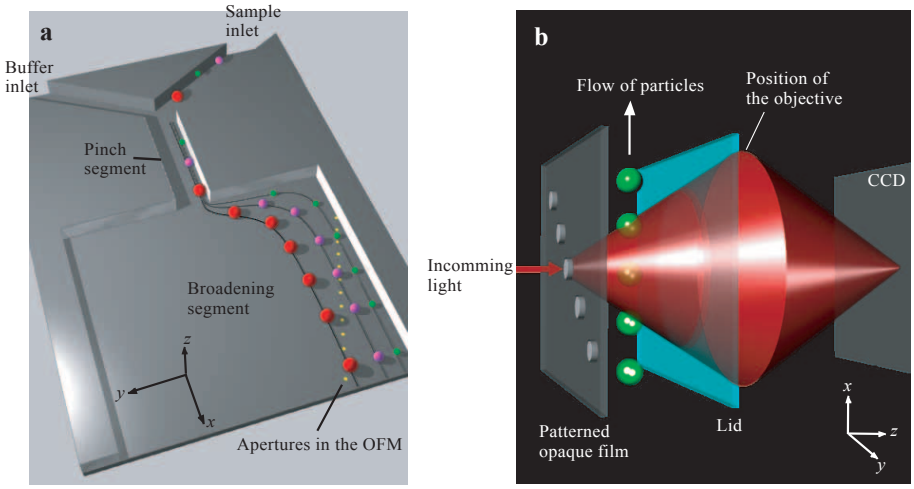

Fig. 1. (a) Principle of pinched flow fractionation (PFF) with an integrated optofluidic microscope (OFM) located in the broadening segment. (b) Illustration of how transmitted light trough an aperture is effected when particles pass in the channel. The light is collected by an objective, after passing the channel, and redirected to a CCD. The angle of the collected light is defined by the numerical aperture of the objective.

for detection of single nucleotide polymorphisms [14]. The principle of PFF is illustrated in Fig. 1(a). A sample containing particles is introduced from a sample inlet channel into a narrow channel called the pinch segment. The particles are aligned (pinched) against a wall in the pinch segment, regardless of size, using the fluid flow from a buffer inlet channel. As the particles move into a wider channel, the broadening segment, the distance from the channel wall to the center-of-mass of the particles is amplified and the particles are separated according to size [10, 15, 16]. When the separated microspheres pass the broadening segment they affect the transmission of light through the apertures constituting the OFM. The transmitted light from each aperture spreads radially and is collected in a cone with a characteristic angle, due to the numerical aperture (*NA*) of a collector objective, as illustrated in Fig. 1(b). Each particle thus affects the light from apertures over a distance in regards to the width of the channel, *y*-direction, which is much larger than their diameter and depends on their height in the channel, *z*-direction, see Fig. 1(b). This enables detection of two dimensional separation: Size separation in the *y*-direction which occurs in PFF and separation in the *z*-direction in response of an external force. An additional separation parameter can thereby be added to PFF without adding any complexity in the detection. Furthermore, PIV is enabled by knowing the geometry and dimensions of the aperture array (the position in the *x*-direction) and the readout sampling rate.

2. Layout and fabrication of devices

The microfluidic PFF separation devices are defined by thermal nanoimprint lithography in a film of cyclo-olefin copolymer (COC), placed on top of an aluminum (Al) film with periodically arranged circular apertures constituting the OFM. All channels in the PFF device are 12.5 μm deep and range from 11.7 μm (pinch segment) to 400 μm (broadening segment) in width. The apertures in the Al film are designed to be 650 nm in diameter and are placed underneath the broadening segment. The apertures are placed in a line, which is tilted relative to the flow direction, *x*, in the broadening segment. The center-to-center distance between the apertures are 14 μm in the *x*-direction and 650 nm in the perpendicular *y*-direction. Two lines, each of

#118773 - $15.00 USD Received 22 Oct 2009; revised 8 Feb 2010; accepted 11 Feb 2010; published 17 Feb 2010
(C) 2010 OSA

307 apertures, are subsequently positioned in the broadening segment along its length, covering the full length and half of the width. The first line of apertures is sufficient to determine the $x(t)$, y and z position of separated particles, and diffusion can be measured comparing with detection at the second line. An illustration of the design is shown in Fig. 2(a) and the fabrication process is described below.

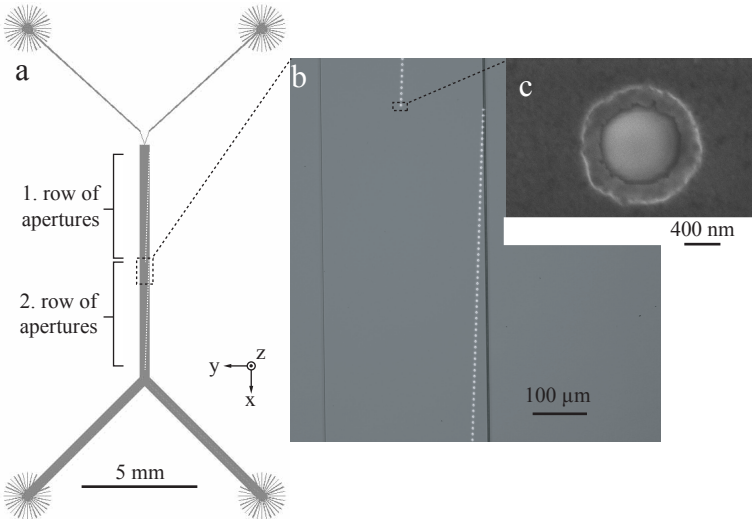

Fig. 2. (a) The device layout. (b) A microscope image of a finished device with backside illumination. The OFM apertures appear as white dots. (c) Scanning electron microscope image of an aperture. The footprint of the isotropic aluminum etch is clearly visible.

A 4 inch borofloat glass wafer (JinSol, Seul, Korea, www.all4semi.com) is used as the substrate. The glass wafer is cleaned in a mixture of 75 % sulfuric acid (H_2SO_4) and 25 % hydrogen peroxide (H_2O_2), rinsed in water and left in an oven at 250 °C over night - all to promote adhesion of Al. 150 nm Al is electron beam deposited (QCL 800,Wordentec, Devon, England, http://www.wordentec.com) on the clean borofloat glass wafer, and a 450 nm thick layer of a positive electron beam sensitive resist (ZEP520A, Marubeni Europe Plc, London, England, http://www.europe.marubeni.com) is spin coated on the Al. Apertures are defined in the resist by an electron beam writer (JEOL-JBX9300FS) and the exposed resist is developed in ZEP-N50 (Marubeni Europe Plc, London, England, http://www.europe.marubeni.com). The Al underneath the openings is etched at an ultra-sound treatment in a mixture of 25 % MF322 (Candor Kemiske A/S, Vejle, Denmark, http://www.candordenmark.dk) and 75 % water. A SEM image of an aperture in the Al film is shown in Fig. 2(c). As seen from Fig. 2(c) the Al etch is isotropic, so short over-etching results in enlargement of the aperture diameter compared to the designed diameter of 650 nm. The aperture diameter of all fabricated devices was measured to range from 650 nm to 850 nm, with an average diameter of 750 nm. At this point the OFM is finished and the PFF device is defined on top of the OFM. A 20 μm COC layer (mr-I T85-20XP, Micro resist technology GmbH, Berlin, Germany, www.microresist.de) is spin coated on the patterned Al layer and the device structures are thermally imprinted in the COC layer leaving a residual layer at the apertures of $8\pm0.1\,\mu$m. Afterwards, inlet and outlet holes are powderblasted and finally the structures are sealed with a borofloat glass lid [17]. The fabrication process of PFF devices is further described in [14]. A microscope image of the fabricated device with backside illumination is shown in Fig. 2(b).

#118773 - $15.00 USD Received 22 Oct 2009; revised 8 Feb 2010; accepted 11 Feb 2010; published 17 Feb 2010
(C) 2010 OSA

3. Methods

The experimental setup is illustrated in Fig. 3. The device is mounted on a holder which fits into the setup and contains fluid connections to the device. A white Halogen light source (Nikon, Surrey, United Kingdom, http://www.nikoninstruments.com) is used to illuminate the apertures. The transmitted light from the apertures is collected with an 10x objective (NA=0.3 in air, Nikon, Surrey, United Kingdom, http://www.nikoninstruments.com) and detected by an EM-CCD camera (Cascade 512II, Photonics, Tucson, United States, http://www.photomet.com), although the electron-multiplication capability of the camera is not used throughout the measurements.

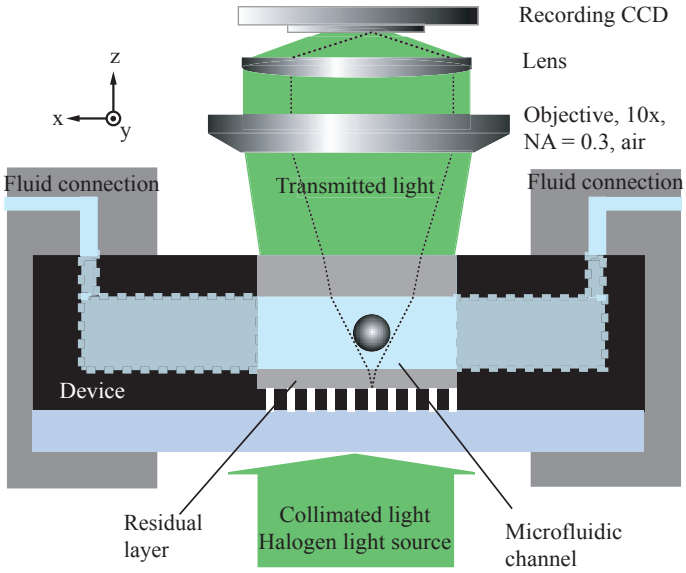

Fig. 3. Cross-sectional illustration of the measuring setup. A device is mounted in chuck width fluid connections. The backside of the device is illuminated by collimated light, and the part that is transmitted through the apertures in the device is collected by a 10x air objective (NA = 0.3), focused by a lens onto a CCD.

Each aperture appears as a white spot consisting of several pixels on the CCD image. When a movie of the transmission is recorded, all apertures are identified in the first image. Here, both the position and number of pixels of each aperture is defined. For all subsequently images, the intensity from each aperture is summed over the relevant pixels. As a result the transmission versus time for all apertures is recorded. An example of such readout over 9.4 s is shown in Fig. 4(a). Here five microspheres passes the aperture. A reference image also of 2.1 μm pinched polystyrene (PS) microspheres passing the OFM at a similar time interval, is shown in Fig. 4(c). Only the transmitted light from each aperture within a solid angle, defined by the *NA* of the objective, is collected, see Fig. 1(b). Therefore, the dip in transmission caused by a passing microsphere depends on the overlap with the cone of light. For a specific z position a maximum dip occurs at the aperture which is best aligned with the center of the sphere. In addition, the microspheres influence the transmission from a number of apertures that cover a distance which is larger than the microsphere diameter. This effect is seen in Fig. 4(b), which shows the transmission through 9 holes, corresponding to 5.9 μm, as a 2.1 μm microsphere passes.

With data as those shown in Fig. 4(a) and 4(b) the $x(t)$, y and z position of a passing microsphere as well as its velocity can be determined as described in the following sections. Further-

#118773 - $15.00 USD Received 22 Oct 2009; revised 8 Feb 2010; accepted 11 Feb 2010; published 17 Feb 2010
(C) 2010 OSA

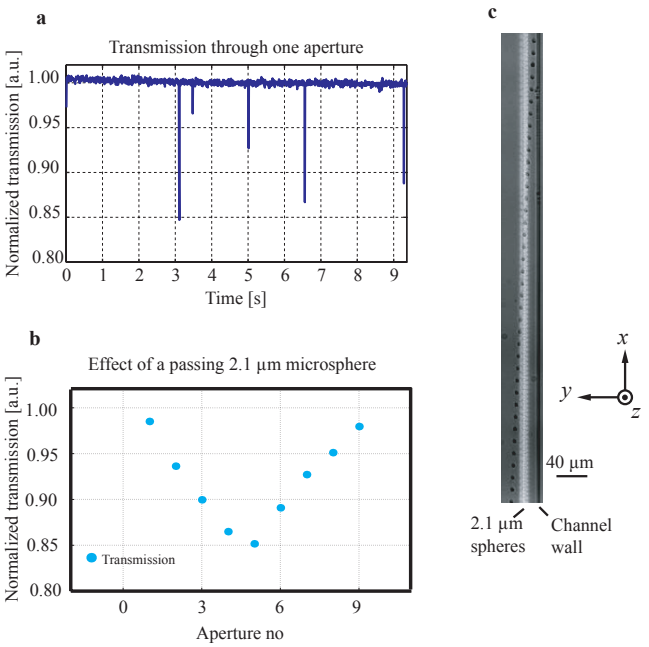

Fig. 4. Transmission readout from the OFM. (a) Readout from one aperture as function of time and when 2.1 μm polystyrene spheres passes. (b) Readout from a 2.1 μm microsphere effecting the transmission from several apertures. (c) Reference fluorescence microscope images of 30 pinched 2.1 μm microspheres passing above the apertures. The exposure time of the microscope is long, so the microspheres appears as lines and several microspheres have passed in the image.

more, the expected position- and velocity distribution of passing objects will be introduced and used to validate the 3D resolution of the OFM.

Detection of separated particles

The position $\langle y \rangle$ for the center of mass of each microsphere in the broadening segment is determined from the "transmission versus aperture number" data. One example of such data set is shown in Fig. 4(b). The weighted average of the transmission data is used to find $\langle y \rangle$:

$$\langle y \rangle = \frac{\sum_i y_i (1 - T_i)}{\sum_i (1 - T_i)} \tag{1}$$

Here y_i is the position of the ith aperture and T_i is the corresponding transmission (see Fig. 4(b)).

In accordance with Eq. (1), the accuracy in $\langle y \rangle$ is increasing with increasing number of data points (apertures, i, for which $T_i < 1$) and thereby, as previously mentioned, it depends on the z position of the sphere and the aperture pitch in the y-direction. The lower limit of the accuracy in $\langle y \rangle$ is given by the aperture pitch, 0.65 μm.

In the PFF separation experiment, see Fig. 1(a), the microsphere diameter D determines the distance, y_{wall}, between the center of the microsphere and the channel wall in the broadening segment [10]. Knowing the distance to the channel wall from each aperture, $\langle y \rangle$ is used to determine y_{wall}. The uncertainty of y_{wall} is thereby a combination of two contributions: (1) the above described accuracy in $\langle y \rangle$ ($\leq$0.65 μm). (2) The uncertainty in position of the apertures

#118773 - $15.00 USD Received 22 Oct 2009; revised 8 Feb 2010; accepted 11 Feb 2010; published 17 Feb 2010
(C) 2010 OSA

in the *y*-direction caused by the electron beam writer (20 nm) and misalignment between the apertures and the imprinted microchannel (0.65 μm). Because of fabrication accuracy the microchannel and the apertures are often misalignment in the y-direction. The first aperture in the microfluidic channel that is not affected by the channel wall is therefore defined as $y = 0$, and is determined with an uncertainty equal to the aperture pitch (0.65 μm). By propagation of errors, the uncertainty of y_{wall} is $\leq$0.92 μm.

The expected value of y_{wall} as a function of D is calculated numerically in [16] for spherical objects. This calculation is performed in Comsol Multiphysics, using a finite element method to solve the steady state Navier-Stokes equation. Diffusion is not included in the model. The model will be used later in the result section, to convert the measured y_{wall} values to diameters of the passing microspheres. The size distribution of the microspheres is Gaussian, centered around the nominal diameter with a standard deviation of 5 % (http://www.thermo.com/eThermo/CMA/PDFs/Articles/articlesFile_52060.pdf). Particles are separated in PFF according to how close they can get to the channel wall in the pinch segment, which to a good approximation is given by their radius. Therefore, the distance y_{wall} of a Gaussian size-distributed particle sample will also be Gaussian. The size distribution, results in a standard deviation on y_{wall} which is equal to 0.6 μm, 1.4 μm, 2.0 μm and 3.2 μm for the four bead sizes. In addition, diffusion is equal in all directions and is therefore expected to broaden the original Gaussian distribution. In this work the diffusion length can be calculated using the Stoke-Einstein equation [18], to vary from 0.8 μm to 3.4 μm depending on the microsphere size and the flow rate in the system.

Detecting the z position of particles in the channel

According to Fraunhofer diffraction a planar wavefront with wavelength λ will, after passing an aperture with diameter d, spread radially from the aperture if d is on the same order as λ. This effect, combined with the numerical aperture, *NA*, of the optical system collecting the light, is utilized to determine the height position, *z*, in the channel of a passing particle. In the following, ray-optics, is used as a first approximation to calculate the light propagation from the aperture, through the microfluidic channel and finally into the objective, as shown Fig. 5.

It is assumed that the *NA* of the objective sets the maximum angle of the light collected from the apertures. The maximum angle, α, and the *NA* is correlated by: $\alpha = \arcsin(NA/n)$, where n is the refractive index of the medium in which the light is propagating. Combining this equation with Snell's law ($n_1 sin(\beta_1) = n_2 sin(\beta_2)$, where n_1 and n_2 are the refractive indices of the medium on each side of an interface and β_1 and β_2 is the angle of the incoming and the outgoing light with respect to the normal of the interface.), which describes the refraction of light traveling through an interface, an expression for the height in the channel, *z*, of a passing sphere is derived. *z* is found to depend on the *NA* of the objective, the geometry of the device, the material properties and the distance, 2*s*, over which the sphere will affect the transmitted light from the aperture (see Fig. 5). *z* is given Eq. (2).

$$z = \frac{s - \frac{D}{2} cos\left[\arcsin\left(\frac{NA}{n_f}\right)\right] - r\tan\left[\arcsin\left(\frac{NA}{n_r}\right)\right]}{\tan\left[\arcsin\left(\frac{NA}{n_f}\right)\right]} - \frac{D}{2}\frac{NA}{n_f} \tag{2}$$

Here D is the diameter of the passing microsphere, n_f is the refractive index of the fluid in the channel, r is the thickness of imprinted material on top of the Al film and n_r is the refractive index of the device material.

By collecting data from several separated microspheres passing inside the broadening segment, a histogram of the *z* positions, can be made. This histogram is expected to reflect the distribution of microsphere velocities in the flow direction.

#118773 - $15.00 USD Received 22 Oct 2009; revised 8 Feb 2010; accepted 11 Feb 2010; published 17 Feb 2010
(C) 2010 OSA

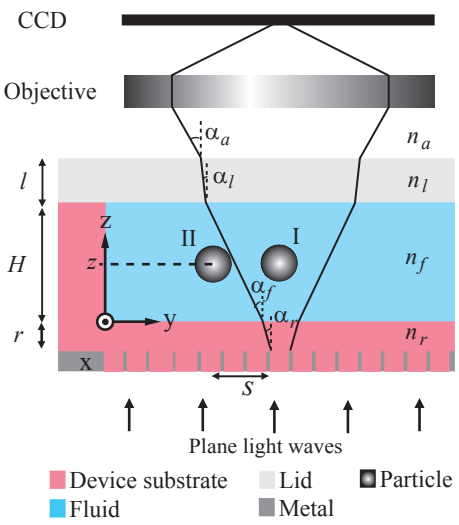

Fig. 5. Cross-sectional view of the propagation of transmitted light from one aperture in the microfluidic device. Two spheres are passing in two different horizontal positions. I: The sphere is located exactly above the aperture, so the transmission dip is at its maximum. II: The sphere is tangent to the cone of light collected from the aperture by the objective, and the transmission from this aperture is unaffected. This sphere effects the transmission from the five apertures to the left. Besides geometries, the refractive indices of air, n_a, the lid, n_l, the fluid, n_f, and the channel material, n_r, is shown in the figure.

In all measurements the flow is pressure driven and the velocity distribution of the fluid is therefore parabolic with maximum velocity in the center of the channel. Providing that the microspheres are distributed evenly in the *z*-direction and follow the flow of the fluid, their expected *z* distribution will also be parabolic. However, as reported in the literature [19], spheres moving in a shear flow as the Poiseuille flow, experience a shear gradient and will, due to minimization of energy in the system, move towards the center of the channel.

The detection accuracy in the *z*-direction, is seen from Eq. (2), to depend on how well s can be determined, the standard deviation of the microsphere radius and the uncertainty of the residual layer thickness. In this study s is found by multiplying the aperture pitch with the number of affected holes of each microsphere divided by two. The accuracy of s, δs, is therefore determined by half the aperture pitch, which is 650 nm. The standard deviation of the microsphere radius is 5 % of its size and the uncertainty of the residual layer is 0.1 μm. By propagation of uncertainties, the detection accuracy in the *z*-direction is found to be limited by δs, and equals 1.4 μm.

The flow velocity in the system was found to be crucial for the success of a measurement. At high velocities only apertures aligned with the central parts of the microspheres yield a transmission dip that is above the detection limit. In this case the information of the *z* position is lost. It is therefore important to operate the system at low velocities. The maximum velocity, at which *z* detection is still possible, is correlated with the minimum exposure time of the used CCD, which in this work is 7.8 ms. The maximum particle velocity was found to be 2 mm/s, corresponding to a total flow rate of 22 μL/h. The implications of this maximum flowrate, in regards to diffusion, is discussed later.

#118773 - $15.00 USD Received 22 Oct 2009; revised 8 Feb 2010; accepted 11 Feb 2010; published 17 Feb 2010
(C) 2010 OSA

Detection of the velocity

The velocity of separated microspheres passing in the broadening segment is determined by recording the time it takes each microsphere to pass the apertures. The velocity is calculated as the slope of a linear function fitted to the *x*-position versus time of each microsphere. The velocity distribution is expected to increase from a minimum velocity for spheres in contact with the wall to a maximum velocity in the middle of the channel, both defined by the parabolic Poiseuille flow profile of the fluid. As discussed above a shear gradient is expected to focus the spheres towards the center of the channel in the *z*-direction, and the velocity distribution is therefore expected to be convex. The accuracy of the velocity is limited by the uncertainty of the linear fit ($< 4\,\%$ of the measured velocity), the uncertainty of the aperture pitch in the *x*-direction (20 nm defined by the e-beam) and the uncertainty in frame rate of the CCD (0.1 μs at 10 MHz readout). By propagation of uncertainties the accuracy of the velocity can be calculated to be up to 4% of the measured velocity, defined by the uncertainty of the linear fit. The velocity should not exceed 2 mm/s, as discussed above, giving an accuracy in the velocity of 0.08 mm/s.

Sample preparation and flow control

In all OFM detection measurements fluorescent labeled polystyrene (PS) microspheres (Thermo Fisher Scientific Inc, Waltham, United states, http://www.thermo.com) with four different average diameters: 1 μm, 2.1 μm, 3 μm and 4 μm are used. These have absorbance maxima at 542 nm and emission maxima at 612 nm. The microspheres are suspended in a carrier buffer consisting of 0.001 wt% Triton X100 in MilliQ water. The microsphere concentration is 0.01 wt%. The microsphere solution is introduced into the device from the sample inlet and carrier buffer without microspheres from the buffer inlet, see Fig. 1(a). As discussed earlier the maximum total flow rate is 22 μL/h. Such small flow rates combined with pinched conditions and a steady supply of sample buffer was achieved with a combined flow rate and pressure controlled setup. The flow in the buffer inlet channels is controlled by syringe pumps (11Plus from Harvard Apparatus) and is varied between 5 μL/h and 30 μL/h. The flow in the sample inlet channel is controlled by an air pump (VP 86 with EU-plug, VWR) and is varied from 5 mbar to 30 mbar corresponding to a flow rate between 0.2 μL/h and 1.2 μL/h.

4. Detection results

Each time a microsphere passes the OFM in the broadening segment the *y* and *z* position as well as its velocity is detected. In the following, we present such detection of separated microspheres. Throughout calibration measurements it was found that the dip in transmission, shown in Fig. 4(a), caused by passing microspheres was doubled when the wavelength of the transmitted light was inside the absorbance range of the microsphere. This observation is important, not only to maximize the signal to noise ratio – which results in better measurements – but also because the absorbance properties of sample particles can be detected and distinguished. At all measurements presented in this article a green filter is introduced between the white halogen light source and the device, see Fig. 3. Thereby, the device is illuminated at wavelengths 535 ± 25 nm.

Separation measurements

Initially, the size separation in PFF, detected with OFM, was compared to detection by fluorescence microscopy. A sample containing fluorescent PS microspheres with average diameters of 1 μm, 2.1 μm, 3 μm and 4 μm was introduced into the device as already described, at a total flow rate of 16 μL/h. The transmission signal was recorded during 47 seconds, resulting in the y_{wall}-position histogram shown in Fig. 6. The y_{wall} position of the microspheres is seen

#118773 - $15.00 USD Received 22 Oct 2009; revised 8 Feb 2010; accepted 11 Feb 2010; published 17 Feb 2010
(C) 2010 OSA

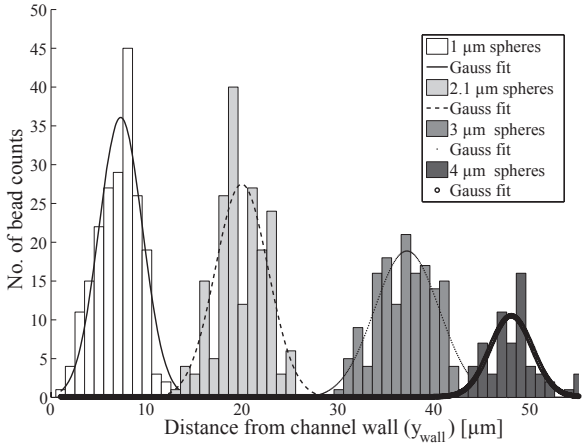

Fig. 6. Histogram of the position in the broadening segment of separated fluorescent labeled polystyrene microspheres with average diameters of 1 μm, 2.1 μm, 3 μm and 4 μm detected by the optofluidic microscope. A Gaussian function is fitted to each of the peaks in the histogram and the position of their maximum together with the standard deviation is given in Table 1.

in Fig. 6 to be well described by Gaussian distributions as expected. The average position and width of the fitted Gaussian functions are therefore good measures of the average position and spreading of each microsphere size in the broadening segment. The earlier described numerical model is used to convert these average values and spreading to microsphere diameters and standard deviations in size, respectively. These values along with corresponding values measured by fluorescence microscopy are listed in Table 1.

Table 1. Measured diameter, D, and standard deviation in diameter,$\sigma(D)$, of the separated microspheres (1 μm, 2.1 μm, 3 μm and 4 μm delivered with a standard deviation in size of 5%). The numerically model (see text) is used to convert the distance from the channel wall to the center of the microsphere in the broadening segment and the spreading, detected by OFM and fluorescence microscopy to diameters and the corresponding standard deviations. The model does not include diffusion, which is the reason for the large deviation between the measured standard deviations and those given by the manufacturer of the microspheres.

	$\langle D\rangle$	$\sigma(D)$	$\langle D\rangle$	$\sigma(D)$	$\langle D\rangle$	$\sigma(D)$	$\langle D\rangle$	$\sigma(D)$
Microsphere specs [μm]	1.0	0.05	2.1	0.11	3.0	0.15	4.0	0.20
PFF with fluor. [μm]	1.0	0.26	2.4	0.46	3.6	0.52	4.3	0.35
PFF with OFM [μm]	0.9	0.26	2.2	0.52	3.6	0.54	4.3	0.36

As seen in Table 1, the microsphere diameters measured by fluorescence microscopy and OFM are in good correspondence. The minor deviations are within the uncertainty given by the measuring method of the y_{wall} position (described earlier). The measured diameters and standard deviations are also seen to be larger than those given by the manufacturer of the microspheres. The numerical Comsol model overestimates, as described in [16], the diameter for a given value of y_{wall}. This is the cause of the deviation in diameter. In addition, diffusion is not included in the model. The large deviation in the defined and measured standard deviations is a result of diffusion, which is seen to limit the performance of the system. The total flow rate in

#118773 - $15.00 USD Received 22 Oct 2009; revised 8 Feb 2010; accepted 11 Feb 2010; published 17 Feb 2010
(C) 2010 OSA

the system should therefore be as large as possible, but can not be larger than 22 μL/h without compromising the detection. In the present system, diffusion is an important limiting factor of the separation.

In Fig. 6 it is observed that the number of detected microspheres decreases with increasing diameter. This is expected, as for a constant solid content (0.01 wt%) the number of spheres per volume decreases with increasing diameter.

z position and velocity measurement

In all presented z position and velocity measurements, the microspheres were introduced one size at the time. The solid concentration of the microsphere sample is 0.01 wt%, but as it enters the pinch segment it is diluted 60 times to approximately 0.00017 wt%, which is the concentration in the broadening segment. The average distance between passing microspheres is then 26 μm, and it is reasonable to assume that particle perturbation of the flow has no significant effect on subsequently passing particles. For each passing microsphere the total number of apertures at which the transmission was affected, was recorded. The number of affected apertures was converted by Eq. (2) (NA = 0.3, n_f = 1.33, n_r = 1.5 and r = 8 μm) to a position in the z-direction. The result of two measurements, with 1 μm microspheres and 2.1 μm microspheres, is shown in Fig. 7(a) and 7(b) as histograms of the z_1 position. In addition, the time each microsphere affected the transmission through the apertures was recorded and, in combination with the known x position, converted into a velocity of the microspheres. The measured velocities of the same measurements is shown in Fig. 8(a) and Fig. 8(b).

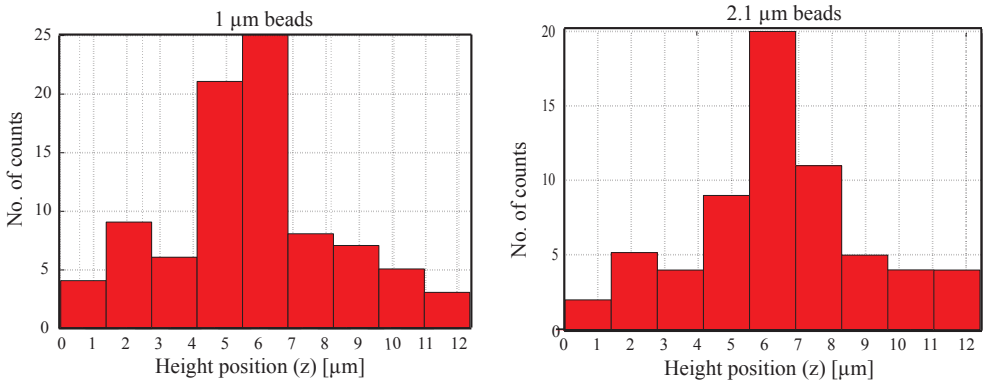

Fig. 7. Histogram of the height position of 1 μm and 2.1 μm pinched fluorescent labeled PS microspheres. The channel height is 12.5 μm.

The total flow rate in the measurement with 1 μm microspheres is 9 μL/h corresponding to an expected minimum velocity v_{min} equal to 0.12 mm/s and a maximum velocity v_{max} equal to 0.75 mm/s. At the measurements with 2.1 μm microspheres the total flow rate was 11 μL/h corresponding to v_{min} = 0.24 mm/s and v_{max} = 0.93 mm/s. The minimum velocity is calculated at a distance to the channel floor of roof corresponding to the radius of the microspheres. However, it should be noted that these calculated values are the velocity of the fluid. The values are indicated as vertical solid lines in the graphs of Fig. 8 and is seen to agree well with the measured microsphere velocities. In Fig. 8, a plot of the velocities calculated from the z-position data in Fig. 7, under the assumption that they follow a parabolic velocity profile with the above derived maximum velocities, is added. As seen in Fig. 8, the measured z positions are in good correspondence with the measured velocities. Furthermore, it is seen from the graphs in Fig. 7 and 8 that the spheres are not following the parabolic flow profile of the fluid, but are forced

#118773 - $15.00 USD Received 22 Oct 2009; revised 8 Feb 2010; accepted 11 Feb 2010; published 17 Feb 2010
(C) 2010 OSA

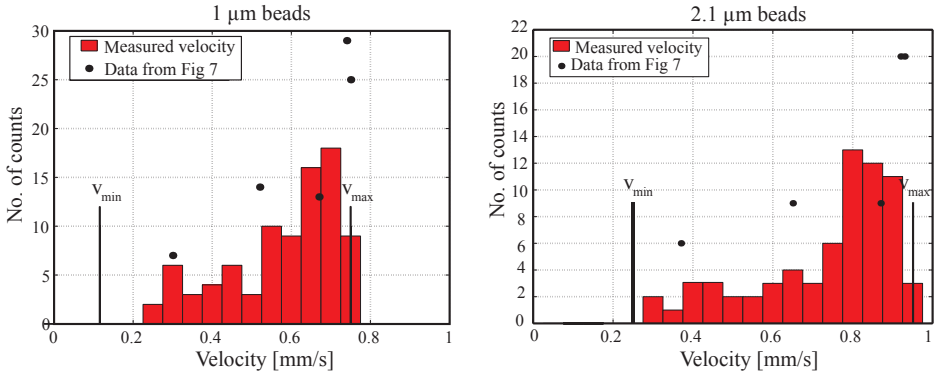

Fig. 8. Histogram of the velocity of 1 μm and 2.1 μm pinched fluorescent labeled PS microspheres. The vertical lines indicate the expected minimum, v_{min}, and maximum, v_{max}, velocity of the carrier fluid.

towards the center of the channels by shear forces as discussed in the method section.

5. Conclusions and outlook

In this paper an optofluidic microscope (OFM) is integrated into a microfluidic separation device based on pinched flow fractionation (PFF). The device has been demonstrated for: 1) in-plane detection of size separated microspheres ranging from 1 μm to 4 μm in diameter with an accuracy of $\leq$0.92 μm 2) out-of-plane detection with an accuracy of 1.4 μm and 3) particle image velocimetry (PIV) with an accuracy of 0.08 mm/s. In all measurements the results were in good correspondence with results obtained by fluorescence microscopy and with the theoretical expectations. An important point to notice is that tumbling of sample particles does not effect the effectiveness of OFM detection in the presented application, contrary to earlier demonstrated applications.

Throughout this work detection along the flow direction has only been used for finding the velocity of passing microspheres. However, separation detection along the flow direction could be used successfully in field flow fractionation (FFF) based separations. Detection of different absorption properties using the OFM was demonstrated in this article but not further investigated. However, this would be interesting in regards to effective on-chip microsphere suspension arrays.

#118773 - $15.00 USD Received 22 Oct 2009; revised 8 Feb 2010; accepted 11 Feb 2010; published 17 Feb 2010
(C) 2010 OSA